

---

## **EFFECT OF CONFINEMENT ON THE FRACTURE BEHAVIOR OF CONCRETE UNDER COMPRESSION**

**K. M. Nemati and P. J. M. Monteiro**

Department of Civil Engineering

Division of Structural Engineering, Mechanics, and Materials

University of California at Berkeley

Berkeley, California 94720, U.S.A.

### **Abstract**

This paper presents the results of experimental studies of the fracture behavior of concrete under compression. Cylindrical specimens of concrete were subjected to testing under uniaxial and confined compression. An alloy with a low melting point was used to impregnate the cracks and pores in the specimen. At the stress of interest, this alloy was solidified to preserve the stress-induced microcracks as they exist under load. Such a technique not only allows one to observe the microcracks as they exist under load, but also facilitates observing the microcracks in three dimensions. Scanning electron microscopy (SEM) was employed to capture images from the cross sections of the concrete specimens. A comprehensive image analysis was performed on the cracking pattern developed in the concrete samples. Direct measurements on backscatter electrons (BSE) images was performed on the computerized images to determine the crack orientation, density, and length of the compressive stress-induced microcracks in concrete and the effect of confinement on microcrack behavior.

# 1 Introduction

The preservation of stress-induced structure and the identification of cracks induced by loading and unloading are important to understand the mechanisms for the generation, propagation and interaction of stress-induced microcracks in complex systems such as concrete. It is important to understand how the formation, growth and interaction of microcracks leads to macrofracture, which are usually the form of failure observed in engineering practice. This paper presents direct observations of the size, orientation and interaction of microcracks in concrete specimens as they exist under load. The proposed method involves the application of a metal in liquid phase, Wood's metal, which has a melting point below the boiling point of water, to preserve the microstructure of stress-induced microcracks in concrete. Used in conjunction with scanning electron microscopy (SEM), it has made possible the detailed observation of microcracks in concrete as they exist under load. Wood's metal was used to study porosity (Yadev 1984), cracks (Pyrak 1988), and fracture (Zheng 1989) of rocks. Nemati (1994) used Wood's metal to study the generation and interaction of compressive stressed-induced microcracks in concrete. The advantage of such an alloy is that it can be injected into voids and stress-induced microcracks at the desired stress level, then solidified at any stage of the experiment to preserve, in three-dimensional form, the geometry of the microcracks induced at any given stage of the experiment.

In this investigation concrete cylinders were tested in compression with various degrees of lateral confinement. While under load, the specimens were impregnated with Wood's metal to preserve the induced cracks. After the metal solidified, sections were cut from the specimens and examined in a scanning electron microscope (SEM). Image analysis was applied to analyze the SEM images and to characterize the quantity and distribution of cracks. The objectives were to determine the shapes and geometry of stress-induced microcracks as they exist under load, and to assess how the density, length, orientation, localization, and behavior of microcracks depend upon the concrete type and confining stresses.

## 2 Experimental technique

The test equipment created to preserve the cracks under applied load is described in detail elsewhere (Nemati 1994, Nemati et al. 1995). Wood's metal is a fusible alloy and in the liquid phase it is nonwetting, with an effective surface tension of about 400 N/m (Yadev et al. 1987). It consists of 42.5% bismuth (Bi), 37.7% lead (Pb), 11.3% tin (Sn), and 8.5% cadmium (Cd). It has a melting point range from 71.1°C to 87.8°C, and is solid at room temperature. Wood's metal has a Young's modulus of 9.7 GPa and a density of 9.4 g/cm<sup>3</sup>.

Five concrete cylinders, 102 mm in diameter by 203 mm long with the mix proportions shown in Table 1. The cylinders were cured for about one year in 100% humidity and a temperature of 23°C. The concrete cylinder ends were ground parallel to one another. Stainless steel wires of 0.3 mm diameter and pre-tension of 130 kN were wound around the concrete cylinder ends to generate biaxial compression. In the partially confined cases the wire was wound one third of the way from each end, at pitch of winding of 4 and 8 pitches per centimeter, and along the entire length at a pitch of winding of 8 pitches per centimeter in the fully confined case.

**Table 1.** Concrete mix design

Material	Quantity/Type
Cement	346 Kg/m <sup>3</sup>
Water	183 Kg/m <sup>3</sup>
Coarse Aggregate	979 Kg/m <sup>3</sup>
Sand	859 Kg/m <sup>3</sup>
HRWR Admixture	10 ml/kg Cem.Wt.
W/C	0.528
Slump	38 mm
Strength	51.7 MPa

A total of five experiments were conducted with conditions as defined in Table 2. Each specimen was loaded to a similar point in the stress strain curve, corresponding to about 80-85% of the ultimate load.

**Table 2.** Experiments conducted

Exp.#	Loading Condition	Load (MPa)	% Ult. Load
1	No Load	10.3*	N/A
2	Uniaxial	34.5	80
3	Partially Confined 1 <sup>†</sup>	41.4	81
4	Partially Confined 2 <sup>‡</sup>	41.4	82
5	Fully Confined	50.6	84

\*restraining load to prevent movement of the specimen during impregnation.

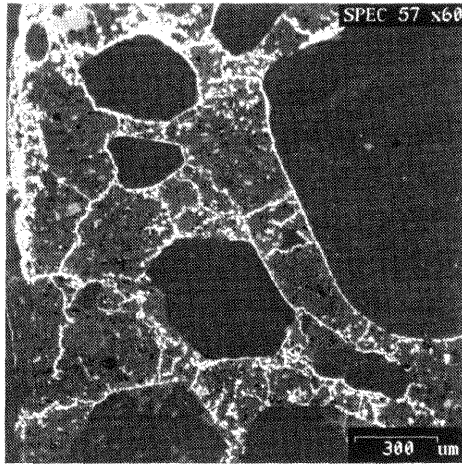
<sup>†</sup>pitch detail: Pitch of winding of 4 pitches per centimeter

<sup>‡</sup>pitch detail: Pitch of winding of 8 pitches per centimeter

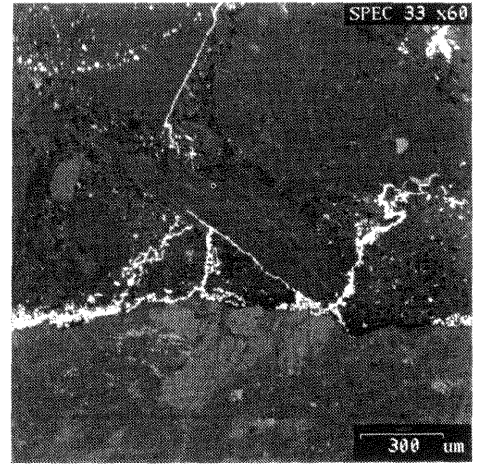
After solidification of the metal each of the cylinders was sectioned along its long axis, using oil as a coolant. One of the half-cylinders was sectioned at the middle, along its diameter. An axial slab, approximately 3 mm thick, was sliced parallel to the direction of the load. Four sections were extracted from the axial slab, two from the mid-line edge and two from the top surface. The specimens were examined using a JEOL JSM-35CF scanning electron microscopy (SEM) in conjunction with a KONTRON SEM-IPS image analyzer.

### 3 Image analysis

The samples were examined in the SEM with backscattered electrons (BSE). The images were acquired by the image analyzer at a magnification of  $\times 60$  and digitized into an array of  $512 \times 512$  pixels with 256 gray levels (1 pixel =  $3.3 \mu\text{m}$ ), 55 images were extracted from each sample. Two typical gray level BSE images are shown in Fig. 1. Fig. 1(a) represents a micrograph of a fully confined specimen from experiment # 5- where the entire length of the specimen was wound by pre-tension wire. Fig. 1(b) is a micrograph of a partially loaded specimen from experiment # 3 where there is uniaxial compression in the center portion and biaxial compression around the extremities, constrained by pre-tension wire. The micrograph in Fig. 1(b) was taken from the confined portion of the specimen and it shows the reduction of microcracks when confinement is applied.



(a)



(b)

**Fig. 1.** Typical BSE images

From the histogram of the distribution of gray levels in a BSE image, the threshold value for discriminating the areas of Wood's metal from other components in the image can be selected. Once the other components in the BSE image, i.e., cementitious phases and aggregates are removed, and after careful image manipulations (Nemati 1994 and Nemati et al. 1995), a skeletonized binary image of the cracks is obtained, which represents the Wood's metal, as shown in Fig. 2.

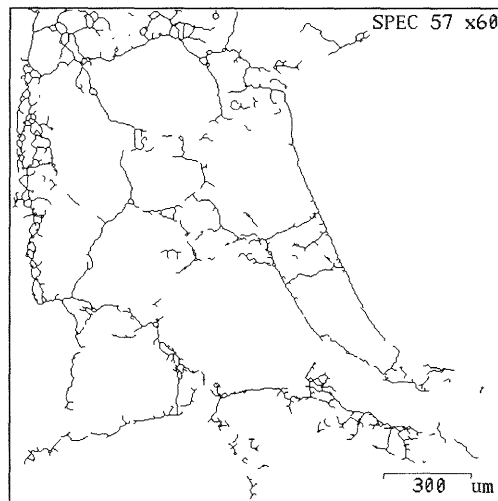


**Fig. 2.** Binary-thinned image of the crack network in concrete

## 4 Results

### 4.1 Microcrack orientation

A two-dimensional analysis of the micrographs indicates that most of the microcracks observed were subparallel to the direction of the maximum compression. In all the specimens on which the observations were made, the microcracks were found to exist within a few degrees of the direction of the maximum compression. Confined 1 and confined 2 refer to experiments 3 and 4 respectively. Fig. 3 shows the microcrack orientation for concrete specimens. The degree of orientation obtained for the partially confined specimens were based on the cracks in the confined portion. A three-dimensional analysis, indicates that the cracks are relatively isotropic at a microscopic level; partly due to the domination of interfacial cracks, which must be randomly oriented (Nemati et al. 1995).

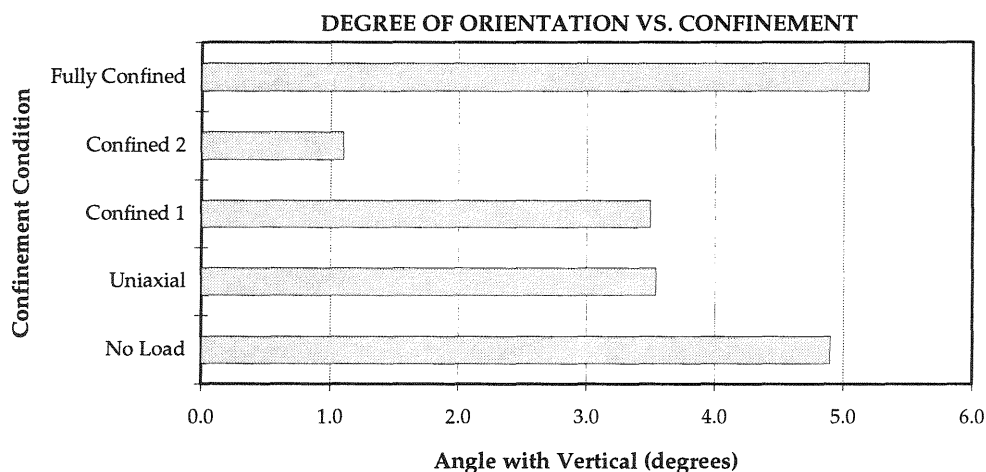


Fig. 3. Average crack orientation

The orientation of microcracks in fig. 3 were algebraic averages of the orientation of the microcracks within each 512×512 pixel square on the corresponding SEM images. The average orientation of microcracks in each of the specimens are listed in Table 3. In these measurements, pore spaces were not counted as microcracks. The number of microcracks per unit of observation area were strongly influenced by confining condition.

**Table 3.** Number, length, and orientation of microcracks

Exp. number	Ave. number of cracks	Ave. length of cracks	Ave angle with vertical
1	60	51.4	4.9
2	86	51.8	3.5
3	65	50.5	3.5
4	37	50.6	1.1
5	35	49.5	5.2

#### 4.2 Microcrack density distribution

The microcrack density distribution,  $\Gamma$ , represents the number of microcracks per unit of observation area. Pore spaces were not counted as microcracks. For a body of volume  $V$  (unit thickness) containing  $N$  cracks with initial cracks of length  $\ell_0$ , the initial crack density parameter  $\Gamma$  is given by:

$$\Gamma = \frac{N\ell_0^2}{V}$$

The crack density parameter  $\Gamma$ , in an image of area  $A$  with  $N$  cracks of length  $\ell_i$ , can be obtained from the following relationship:

$$\Gamma = \frac{\sum_{i=1}^N \ell_i^2}{A}$$

Where:

$\Gamma$  = Crack density parameter

$\ell_i$  = Crack length (mm)

$A$  = SEM image area (512 pixels  $\times$  512 pixels = 2.8358 mm<sup>2</sup>)

Fig. 4 shows the crack density as a function of confinement. From this figure the effect of confinement on crack density is quite evident. The reference specimen (no-load sample) has a relatively high crack

density due to the fact that concrete is heavily cracked even before applying any load (Hsu et al. 1963) and also partly due to the drying process prior to the experiment. Hence, the effective crack density increase for the specimen subjected to applied loads is the difference between the final crack density and the crack density of the no-load specimen. The crack densities for the partially confined concrete cylinders in Fig. 4 are only the crack densities in the confined portion of the samples.

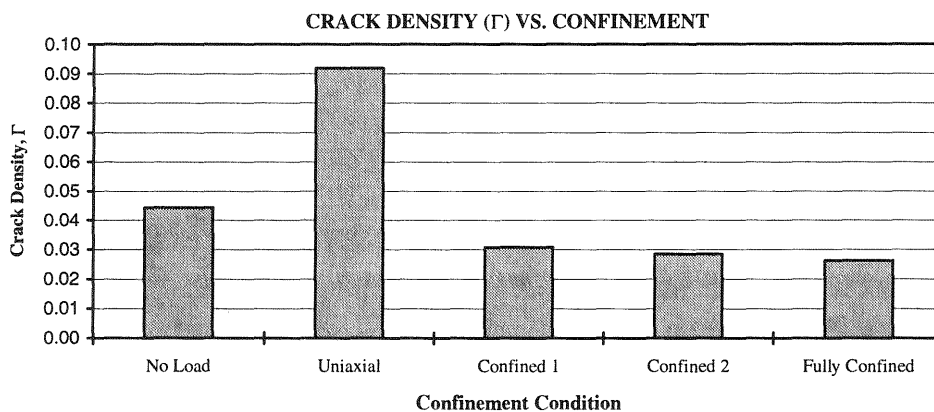


**Fig. 4** Crack density,  $\Gamma$ , as a function of confinement

The specimens subjected to uniaxial compression had the highest crack density. With increasing confining stress, the average crack densities decreased so that the fully confined specimen had the lowest crack density. Both partially confined specimens had very close crack densities.

### 4.3 Microcrack length distribution

The average length distribution of the microcracks strongly depends on the confining stress. In the specimen subjected to uniaxial compression, most of the microcracks propagated to a certain length and then stopped. When confining stress was introduced, the average length of the microcracks decreased, as indicated in Fig. 5. The fully confined specimen, had the lowest crack length.

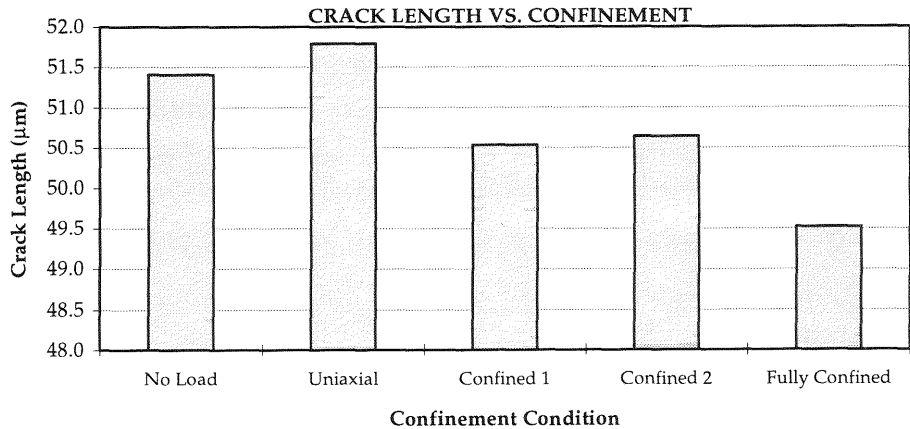


**Fig. 5.** Crack length as a function of confinement condition

## 5 Summary and conclusion

A special experimental technique was developed which made possible the preservation of the compressive stress-induced microcracks in concrete as they exist under applied loads. This technique involved injecting a molten-metal alloy into the induced cracks and solidifying it before unloading. By analysis of BSE images, various measurements of the crack orientation, density, and length were performed. Microcrack orientation, density, and length were strongly influenced by the amount of confining stress to which they were subjected. Measurements of the orientation indicated that the cracks were subparallel to the direction of maximum applied stresses. Microcrack density decreased as the confining stress increased. The specimen subjected to uniaxial compression had the highest crack density, and the specimen loaded under fully confined condition had the lowest value. The average length was longest in the uniaxial experiment, and shortest in the fully confined experiment. Confinement dramatically decreased the crack density observed in the loaded samples. Confinement decreased the average crack length, as measured on the two dimensional sections.

## 6 References

- Hsu, T. T. C.; Slate, F. O. (1963). "Tensile Bond Strength Between Aggregate and Cement Paste or Mortar," *Journal of the American Concrete Institute, Proceedings*, 60, 4, 465–486.
- Nemati, K. M. (1994). "Generation and Interaction of Compressive Stress-Induced Microcracks in Concrete." *Ph.D. Thesis*, University of California at Berkeley.
- Nemati, K. M., Monteiro, P. J. M., Cook, N. G. W., Myer, L. R. (Submitted 1995). "New Method for Studying Stress-Induced Microcracks in Concrete Using Molten Metal Alloy." *Materials and Structures*.
- Pyrak, L. J. (1988). "Seismic Visibility of Fractures." *Ph.D. Thesis*, University of California at Berkeley.
- Yadev, G.D.; Dullien, F. A. L.; Chatzis, I.; and Macdonald, I. F. (1984). "Microscopic Distribution of Wetting and Non-Wetting phases in Sandstone During Immiscible Displacements," *Paper SPE 13212, presented at the 1984 SPE Annual Technical Conference and Exhibition*, Dallas, Texas.
- Zheng, Z. (1989). "Compressive stress-induced microcracks in rocks and applications to seismic anisotropy and borehole stability," *Ph.D. Thesis*, University of California at Berkeley.